J. Geophys. 40, 37–56, 1974

Original Investigations

Statistical Analysis of the Pitch Angle Distribution of Magnetospheric Solar Protons during Geomagnetic Activity

M. Scholer, G. Morfill, and D. Hovestadt

Max-Planck-Institut für Physik und Astrophysik,
Institut für extraterrestrische Physik, Garching

Received September 17, 1973

Abstract. The pitch angle distributions of energetic solar protons in the pseudo-trapping region were used in order to examine magnetospheric processes. Temporal and spatial variations of these processes should give insight into the magnetospheric dynamics. Data from two instruments (viewing angle perpendicular and 45° with respect to the local geomagnetic field) on board the low altitude polar orbiting satellite GRS/Azur give a rough measure of the pitch angle distribution of energetic solar protons ($1.5 < E < 2.7$ MeV) over the polar cap. For several solar particle events the ratios of the counting rates of the two instruments were ordered according to invariant latitude, magnetic local time and geomagnetic activity. The geomagnetic activity was expressed by the time phase relative to the expansion of isolated substorms and the H-component of the magnetic field at a near midnight auroral station. Thus the analysis shows substorm-related effects on energetic particles in the pseudo-trapping region.

Key words: Magnetosphere — Solar Protons — Substorms.

Introduction

Measurements of energetic solar particles over the earth's polar caps have been extensively reported in the literature. The main interest in this subject is due to the fact that these measurements can reveal the topology of the geomagnetic tail.

As far as energetic solar protons are concerned the low altitude polar cap can essentially be divided into three regions: The open field line region, where entry is mainly from the tail, the pseudo-trapping region between the last closed field line and the last closed drift shell and the stable-trapping region at latitudes below the last closed drift shell. Whereas the latitudinal flux structure in the open field line region is closely related with the entry of solar protons into the magnetosphere and thus with the topology of the magnetosphere, investigation of the pitch angle distribution of solar protons on closed field lines and the position of the cut-off latitude can contribute to the understanding of magnetospheric dynamics.

Paulikas *et al.* (1968) and Blake *et al.* (1968) have inferred the quasi-trapped nature of solar protons from their pitch angle distribution peaked at 90° to the geomagnetic field line. Flindt (1970) has identified the pseudo-trapping region boundary within which a double loss cone decreases the counting rate of a low altitude omnidirectional detector, by the 'edges' in the counting rate profiles thus produced. However, as shown by Morfill (1973a), quasi-trapped particles do not necessarily have an anisotropic pitch angle distribution. Breakdown of the first adiabatic invariant in the strongly curved field line regions near the last closed field line leads to an effect which cannot be differentiated from strong pitch angle scattering by a low altitude satellite detector. In addition resonant scattering of the particles with hydromagnetic waves during magnetically disturbed times can lead to pitch angle redistributions.

Dispite the large amount of polar cap proton data reported in the literature, detailed investigation of their pitch angle distribution and cut-off variation during times of geomagnetic activity is relatively rare. Imhof *et al.* (1971) found a significant decrease of the cut-off latitude with increasing K*p*, which confirmed previous findings by Paulikas *et al.* (1970). Bewick *et al.* (1970) compared the solar proton cut-off with the high latitude electron boundary during substorm activity. They found that solar protons become trapped and are transported to lower latitudes during magnetospheric substorms. Williams and Heuring (1973) have shown cut-off variations of solar protons during a large geomagnetic storm, without, however, commenting on the detailed time variation of these cut-offs. They found a development of an isotropic loss cone distribution from an anisotropic distribution on the day side during the development of the symmetric ring current, indicating strong pitch angle diffusion.

The present report attempts to investigate the solar proton pitch angle distribution during geomagnetically active times on a statistical basis. Several solar particle events have been observed from December 25, 1969, to April 7, 1970 by the low altitude polar orbiting satellite GRS-A Azur. The events were subdivided according to the substorm activity expressed by the time phase relative to the expansion and by a signature level given by the depression of the *H* magnetometer component of a near-midnight auroral station.

Instrumentation

The data presented in this paper were taken with two identical particle telescopes on the dawn-dusk polar orbiting satellite GRS-A Azur (inclination 102.94°, perigee 383 km, apogee 3145 km, period 122 min.) The satellite is magnetically stabilized. The two proton-alpha particle telescopes (88/1 and 88/2) are oriented one perpendicular and one at an angle of 45°

(88/2) with respect to the local geomagnetic field vector. In the northern hemisphere telescope 88/2 points upwards. Only data from the lowest energy channel ($1.5 \leq E_p \leq 2.7$ MeV) are used for this investigation. In addition data from an omnidirectional proton-electron detector (93/1) were used in order to indicate the location of the 1 MeV electron radiation belt. A detailed description of the experiments and an analysis of the calibration measurements are published in Achtermann *et al.* (1970).

The half opening angle of each of the two detectors is 22° and the sizes of atmospheric loss cones are typically ~37° for the satellite altitude over the northern polar cap during the time of the observations. Therefore, instrument 88/2 points partially into the upper atmospheric loss cone if there is a double loss cone distribution, whereas instrument 88/1 is unaffected. The reduction in measured counting rate for the 88/2 detector relative to 88/1 is approximately 28% in the case of sharp loss cones and an isotropic distribution everywhere else. Therefore, we can describe the strength of the scattering processes acting on trapped and quasi-trapped particles by the ratio R = counts in detector 88/1 : counts in detector 88/2. If $R > 1$ we have a double loss cone distribution, if $R < 1$ there is particle precipitation along the field lines and if $R = 1$ the flux is isotropic with the loss cone filled up.

Method of Analysis

The method of analysis is discussed in some detail. This is done so that the reader can assess the statistical significance of the presented data and to give a guideline for possible similar statistical investigations. The ratio R of the counting rates in the instruments 88/1 and 88/2, henceforth designated with c_{90} and c_{45}, were divided into 12 intervals of width $\Delta R = 0.2$ from $R = 0$ to $R = 2.4$. The ratios were then ordered according to invariant latitude Λ, magnetic local time MLT and magnetic activity M. The process to be investigated is substorm activity, expressed by the time phase relative to the expansion and a certain signature level given by the maximum depression of the H-component of the magnetic field at a near local midnight auroral station. Thus in this analysis $M = T$ and B_0. To account for the statistical error at low counting rates, the ratios R are weighted according to their relative error, i.e. the weighting factor is

$$1 - \varkappa(\Lambda, MLT, M, R) = 1 - \frac{1}{\sqrt{c_{90}}} - \frac{1}{\sqrt{c_{45}}} \tag{1}$$

If $\varkappa > 1$ (i.e. the average counting rate < 4 counts/frame) the data were rejected. The weighted frequency of occurrence in a certain Λ, MLT, M, R interval is then

$$N_0(\Lambda, MLT, M, R) = \sum_{l=1}^{k} (1 - \varkappa(l, \Lambda, MLT, M, R)) \tag{2}$$

whereby the summation is taken over all events falling into these Λ, MLT, M, R intervals. For each of the Λ, MLT, M intervals we can construct histograms by plotting N_0 vs. R. From the mean of the distribution, the spread around the mean and from the shape of the histogram, it is possible to draw conclusions about effects which influence the energetic solar particle distributions inside the magnetosphere, i. e. those where the magnetosphere plays an active, dynamic role.

In order to understand these experimental histograms we have to calculate the corresponding theoretical histograms which we would obtain from the statistics of the measurements. In the case of an isotropic pitch angle distribution with no loss cones, this is done in the following way.

From the two counting rates c_{90} and c_{45} we get a mean counting rate

$$\bar{c} = (c_{90} + c_{45})/2 \tag{3}$$

The probability of measuring a counting rate 'm' in one of the detectors is given by the Poisson distribution:

$$P(m) = \frac{\bar{c}^m e^{-\bar{c}}}{m!} \tag{4}$$

We now require the probability χ of obtaining a ratio R of the counting rates c_{90} and c_{45}, where $R_0 < R \leq R_1$. χ is given by

$$\chi(R_0 < R \leq R_1) = \sum_{\mathrm{m}} \sum_{\mathrm{n}} P(m)\, P(n) \tag{5}$$

where the summation is taken over all counting rates m and n, so that

$$R_0 < \frac{m}{n} \leq R_1 \tag{6}$$

It has been assumed in (5) that the particle distribution is isotropic with the mean counting rate in each detector given by $\bar{c}$.

Multiplication of χ with the weighting factor $\varkappa$ and summation over all events gives finally the theoretical histogram 'N_T' for the case of an isotropic pitch angle distribution.

Fig. 1 shows $\chi(R)$ for four different values of $\bar{c}$. As one would expect, the distribution gets sharper with increasing mean counting rate. Typical counting rates of the measurements reported here are in the order of ~ 50 counts per 10 sec. An interesting feature of this analysis is the double peak structure at low values of mean counting rate $\bar{c}$. This is an entirely real phenomenon and arises out of the probability of the ratio $R = \frac{c_{90}}{c_{45}}$ lying within the limits R_0 to R_1 when c_{90} and c_{45} are quantised values.

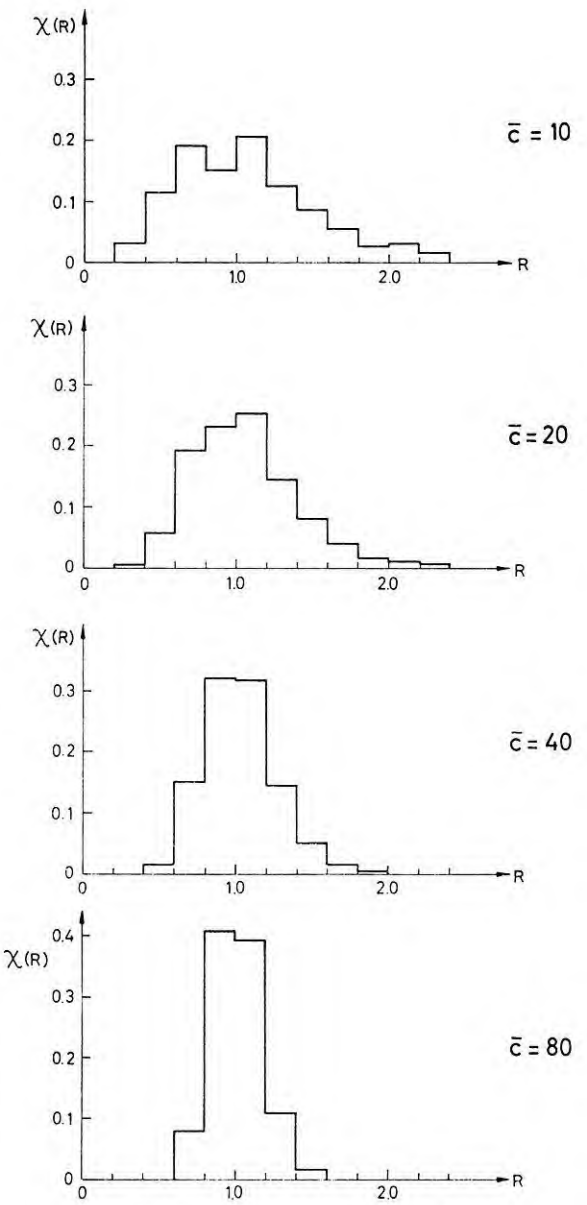

Fig. 1. Theoretical histogram of the probability $\chi(R)$ of obtaining a ratio in counting rates $c_{90}/c_{45} = R$. Probabilities are added in parameter blocks $\Delta R = 0.2$. Probability distributions are shown for four different mean counting rates $\bar{c}$

Aims of the Statistical Analysis

The method which we have developed fulfills the aims of our analysis, which are firstly, to formulate the pitch angle distribution problem in a manner which gives the desired information about the spatial dependence (Λ, MLT) and the activity — temporal dependence (B_0 and T), and secondly to compare the observed distributions (in the form of histograms) with a theoretical calculation of isotropic particle fluxes. It thus becomes possible, to decide on the basis of measurements and theoretical histograms whether the observations at a given position, time and magnetic activity correspond to an isotropic distribution in pitch, a double loss cone distribution, a trapping distribution or precipitation into the atmosphere. The spatial and temporal variation can then be used to find out if on average any one of these processes is predominant at a given place or time, and thus to associate the process with the corresponding magnetic activity.

This type of information can only be obtained with a statistical analysis, and clearly it is important to reduce the wealth of variable parameters to manageable levels without masking and encoding the information content of the data too drastically. In our particular case we are also limited by the detector configuration, but we feel that a substantially more detailed pitch angle resolution than ours would need to be simplified to a similar parameter such as our ratio $R = \frac{c_{90}}{c_{45}}$ in order to avoid too much complexity. Improvements to our analysis can be obtained by eg. using $R = \frac{c_{90}}{c_0}$, larger geometric factors (and correspondingly larger counting rates) and observation of more events, i.e. increasing the statistical weight. It is for this reason that we have described the method of analysis in perhaps greater detail than otherwise necessary.

In order to evaluate the observed pitch angle distributions in the context of possible mangetospheric processes, which may be acting on the particles, it is necessary to understand the normal spatial variation of these distributions when no influences other than the field topology itself (assumed to be static) exist. Some comments on this are made by Morfill (1973b).

Normal Pitch Angle Distributions

In the open field line region, there is only a single relatively sharp loss cone, which can not be observed by our two detectors 88/1 and 88/2 due to their orientation in the satellite. The pitch angle distribution is isotropic outside this loss cone, which is well approximated by projection to the satellite of a zero flux level, which is due to atmospheric absorption at altitudes of 100 km.

In a invariant latitude band between 3° to 5° wide, at latitudes just below the last closed field lines, Morfill (1973a) has shown that 1 MeV protons do not conserve the first adiabatic invariant. This results in a single loss cone distribution at low altitudes, although the detector is on closed field lines. The particle intensity here is then similar to that just on open field lines near the last closed field line.

At all latitudes below this boundary, the particles exhibit a double loss cone distribution, the second (upper) loss cone being formed by atmospheric absorption at the conjugate point in the other hemisphere.

Since the breakdown of the first invariant extends into the closed drift shell region at midnight (Morfill, 1973a) it must be relatively easy for particles to find access into the trapping region at these localised positions. Since these particles are able to drift around the earth more than once, a trapping distribution may be set up (Roberts, 1969), even at quiet times. This trapping distribution is characterised by larger loss cones than the double loss cone distribution, and relatively smooth pitch angle-intensity profiles.

It is clear that the boundaries of these pitch angle distribution 'regions' in this 'normal' picture are closely related to (and in general a few degrees below) the 40 keV and 1 MeV electron boundaries.

We shall now give a brief phenomenological account of the modification of these 'normal' distributions described. More detailed descriptions can be found in eg. Morfill, (1973a,b) Bewick *et al.* (1973).

Strong Pitch Angle Scattering

Leaving aside the question of the sources of such scattering, we assume that scattering can vary spatially in longitude and latitude. For a given drift shell, the effect of a localised region of strong pitch angle scattering, is to isotropise the equatorial particle distribution, filling up the atmospheric loss cones in a time short compared to the particle bounce period, τ_b.

$$\tau_b = 2 \int_{M_S}^{M_N} \frac{ds}{V_{\|}} \tag{7}$$

where M_N and M_S are the northern and southern mirror points, ds is the element of length along the field line in the given drift shell, and $v_{\|}$ is the component of particle velocity parallel to the field.

$$\tau_b = 3.3 \cdot 10^9 \frac{L}{v} (1 - 0.43 \sin \alpha_0) \tag{8}$$

τ_b is in seconds, L in earth radii, v in cm/sec. α_0 is the equatorial pitch angle.

Outside this localised region, the particle distribution again becomes double loss cone and possibly trapping. If strong pitch angle scattering exists at all local times, the distribution is isotropic along the whole drift shell.

Weak Pitch Angle Scattering

When weak pitch angle scattering exists, this manifests itself to a low altitude particle detector as an increase in the atmospheric loss cone. Particles which mirror at low altitudes above the atmosphere are scattered into the loss cone and are not replaced, as in the case of strong pitch angle scattering, by particles mirroring near the equator. Consequently, as the particle distribution drifts around in longitude, the loss cone size increases, so that — in the case of positively charged particles — the dawn loss cone is greater than the dusk one.

Precipitation

The definition of precipitation adopted here is simply $c_{45} > c_{90}$, or there are more particles whose mirror points lie below the satellite, at a point along the field line where the magnetic field strength is twice that at the satellite position. This mirror point may lie below the atmospheric cut-off in which case these particles will be absorbed, and the same mya be true for the conjugate point, if the satellite is on closed field lines. In this case, an adiabatic projection of the two satellite directions of incidence (45° and 90° pitch angles) to the equator can be made, in order to asses the shape of the particle distribution at that position. We have

$$\sin \alpha_{90} = \sqrt{2} \sin \alpha_{45} \tag{9}$$

where α_{90} corresponds to the equatorial pitch angle of particles mirroring at the satellite and α_{45} to the particles with pitch angles of 45° at the satellite position.

These 45° particles mirror at $\sim r = 1$, so that

$$\sin^2 \alpha_{45} = \frac{1}{L^3} \tag{10}$$

Thus at eg. $L = 8$:

$$\alpha_{45} \approx 2.5°$$

$$\alpha_{90} \approx 3.5°$$

A difference of only a few percent in the directional proton intensities at these two viewing directions is representative, therefore of a sizeable

anisotropy over a small angular region of the equatorial particle distribution. However, at any intermediate distance, the anisotropy will be less pronounced than described here for the equatorial case.

Spatial Resolution

As mentioned earlier, the statistical method devised here allows us to examine the full spatial distribution of magnetospheric processes which affect the solar proton pitch angle distribution. Clearly, it is necessary, once the expected quiet time behaviour of the spatial variation has been developed, to determine the boundaries between the different regimes.

In Fig. 2 we have shown cross sections of the magnetospheric noon midnight meridian at normal low magnetic activity (a), the substrom build-

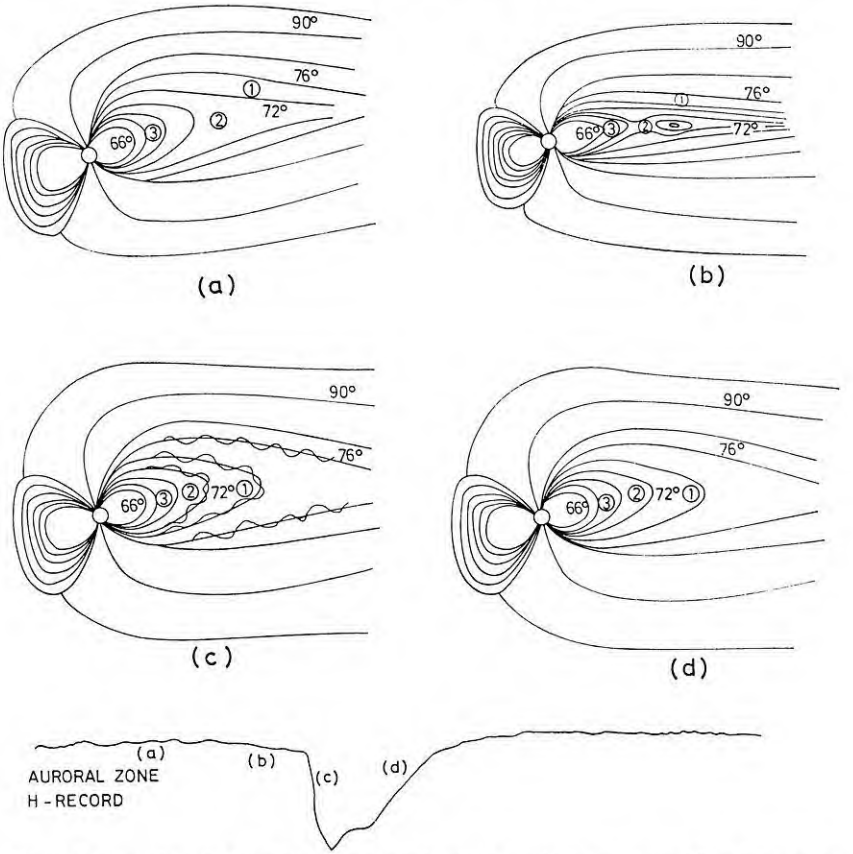

Fig. 2. Schematic field lines in the noon-midnight meridian at normal low magnetic activity (a), the substorm build-up phase (b), the substorm expansion phase (c), and the quiet post substorm phase (d)

up phase (b), the substorm expansion phase within half an hour of the actual expansion (c) and the quiet post substorm expansion phase (d). The times to which these figures refer are shown schematically in relation to a typical isolated substorm auroral zone H-record magnetogram. These figures are based partially on the magnetic field observations of Fairfield and Ness (1970).

In (a), the electron trapping boundary occurs at around 68° invariant latitude, and the figure shows the continued reconnection of field lines across the neutral sheet observed by eg. Behannon (1970).

In (b), the electron trapping boundary occurs at around 66°, the magnetic field strength in the tail is greater than in (a) and the plasma sheet moves closer to the earth. Also shown schematically is a neutral sheet magnetic field structure such as proposed on observational evidence by Schindler and Ness (1972).

In (c), the electron trapping boundary occurs at around 72°, although dipole-like field lines extend to about 74°. The magnetotail has expanded and is characterised by this dipole-like topology and low field strengths. Also indicated schematically are magnetic fluctuations such as observed by McPherron and Coleman (1970) with ATS 1. These fluctuations are a common occurrence on the nightside during magnetic substorms. They are compressional in nature and begin shortly after the start of the expansion phase and last for typically 30 minutes to one hour.

In (d), the expansion phase of the substorm is still in progress, but the field fluctuations described in (c) have died down. The electron trapping boundary occurs at around 72°, but the field gradually begins to assume the 'normal' character described in (a).

Regions (1), (2) and (3) indicated in the figure correspond to midnight invariant latitude intervals of 72°—75°, 69°—72° and 66°—69° respectively. The regions sampled by the Azur detector were also grouped in these invariant latitude bands. Due to the asymmetric nature (with respect to the geomagnetic pole) of the high latitude polar cap (eg. Morfill, 1972) these Azur regions might not necessarily correspond to the three regions shown in Fig. 2). The satellite orbit always remained in a narrow magnetic local time band at these latitudes. On the dawn side this was from 3.00 to 5.00 Magnetic Local Time (*MLT*), on the dusk side from 18.00 to 20.00 *MLT*. From the known, or inferred, position of the last closed field line and last closed drift shell at the times a) to d) of Fig. 2, we can deduce the region in space near the midnight meridian sampled by the satellite during its passage through these invariant latitude bands. It is found that the slight asymmetry in the orbits does not produce major dawn — dusk differences. Below we have constructed a table showing the regions sampled by the satellite in the three invariant latitude bands during the different times investigated.

a) – normal magnetosphere

Λ-band	Region sampled
1	open field lines
2	front edge of neutral sheet and nonadiabatic part of pseudotrapping region
3	'stable' trapping within nonadiabatic drift shell region

b) – growth phase

Λ-band	Region sampled
1	open field lines
2	open/front edge of neutral sheet
3	front edge of neutral sheet (nonadiabatic part of pseudotrapping region)

c) and d) – expansion phase

Λ-band	Region sampled
1	front edge of neutral sheet nonadiabatic part (pseudotrapping region)
2	stable trapping region (partly within nonadiabatic drift shells)
3	stable trapping (adiabatic drift shells)

The dusk side invariant latitude bands, where they sample the front edge of the neutral sheet, are reached on the first, or at most the second bounce, so that these particles should retain information about the topology and dynamics of the nightside region near the neutral sheet.

Fig. 3 shows an invariant latitude (Λ), Magnetic Local Time (MLT) plot for case (a), the 'normal' magnetosphere, taken from Morfill (1973a). The regions covered by the orbits in our analysis are indicated, as well as the open field line region (as determined from particle trajectories), the nonadiabatic part of the pseudotrapping region (where strong magnetic field gradients and curvature give rise to nonadiabatic particle motion) and the pseudotrapping region (where particles cannot drift around the earth by more than 360° without being lost, i.e. no closed drift shells) are indicated.

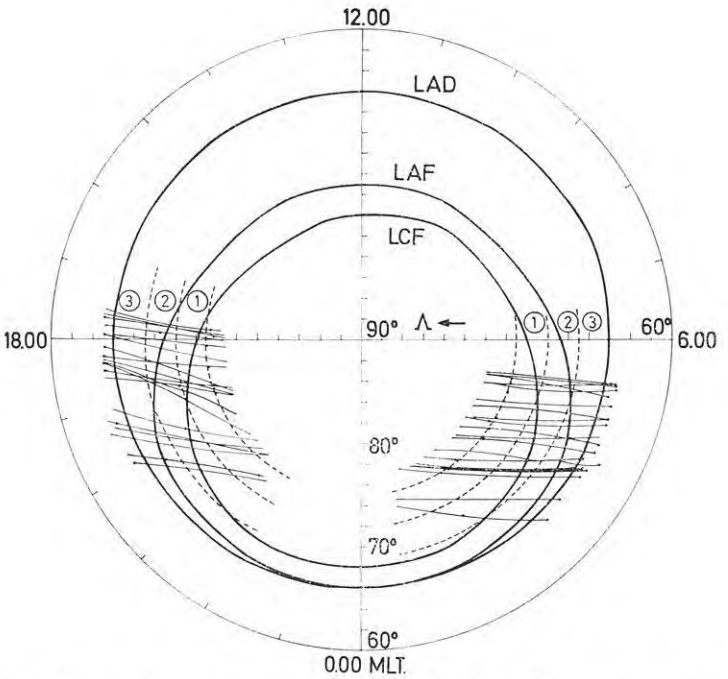

Fig. 3. The regions covered by the orbits in the statistical analysis in an invariant latitude — magnetic local time diagram. Also indicated are the last closed field line LCF, the last adiabatic drift shell LAD and the nonadiabatic part of the pseudotrapping region (between LCF and LAF)

Temporal Resolution

The temporal resolution during this statistical analysis is determined only by the number of orbits available, and the number of isolated substorms. We have chosen a half hourly resolution during the two hours before and after the substorm expansion and then a coarser time-grid. This choice was made mainly because the polar passages of the satellite last for typically 20 minutes, the exact time of the substorm expansion could not be determined very accurately in some cases ($\pm$ 10 minutes), and a better resolution would have decreased the statistical accuracy.

Observations and Discussion

Before presenting the results of the statistical analysis we discuss individual measurements from a single substorm. Fig. 4 shows an example of electron and proton measurements during an isolated substorm on March 29, 1970, at 24.00 UT taken from Häusler *et al.*, 1973. Orbit 1676

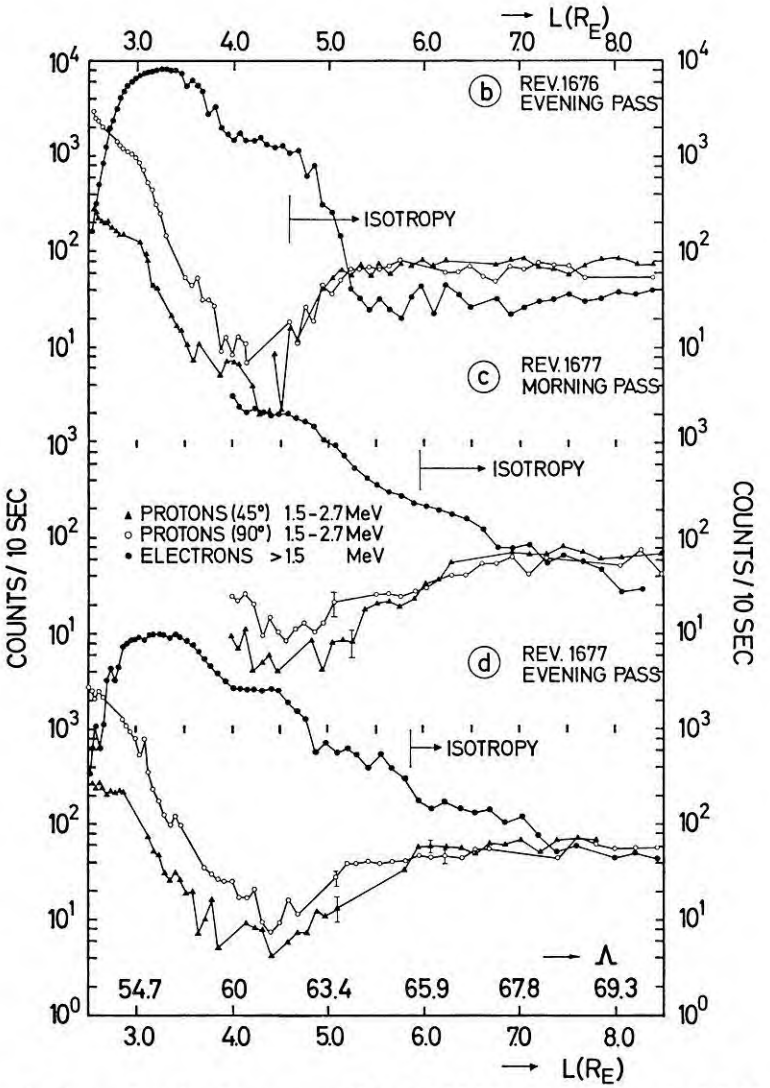

Fig. 4. Trapped and solar protons (1.5–2.7 MeV) and electrons (>1.5 MeV) measured during an isolated substorm on March 29/30, 1970. Proton fluxes are observed in two directions with respect to the local geomagnetic field (indicated by two different symbols). (From Häusler *et al.*, 1973)

was recorded about 30 min before the substorm expansion phase, during orbit 1677 the satellite passed the north polar cap in the recovery phase about 90 min after the substorm expansion. Whereas in the orbit just prior to the substorm expansion the electron belt extended out to $L \sim 5.3$,

it reached up to $L \sim 7$ afterwards. The small radial extent of the elcetron belt during the growth phase of a substorm is generally thought to be due to the following: Field lines from the front side of the magnetopause are transported into the tail (Aubry *et al.*, 1970), resulting in a higher tail field strength, and stronger currents in the neutral sheet. The strong tail field, in turn, opens up the dipolar field lines and stretches them deep into the tail. Particles on these field lines can no longer execute a full drift and the last closed drift shell moves towards lower latitudes. The increase in radial extent of the electron belt after the substorm expansion is understood in the following way: Field lines in the tail reconnect and snap inwards, and the electron trapping boundary moves towards higher latitudes, following the collapse and recapturing or acceleration of electrons on these high latitude closed field lines. This description is consistent with the observations of Ness and Williams (1966) and Williams and Ness (1966) who found a correlation between the tail field strength and the location of the high latitude electron boundary.

As can be seen from Fig. 4 the solar proton flux is isotropic everywhere, within the limits of the counting statistics, before the expansion (Orbit, 1676). In the recovery phase the decrease from the high latitude plateau flux value towards the particle cut-off is more gradual, and the pitch angle distribution is anisotropic between the cut-off at $L \sim 4.5$ and $L \sim 6$.

We now proceed to investigate substorm related effects on a statistical basis. During the time interval from December 25, 1969 to April 7, 1970, 68 substorms were selected during which energetic solar protons were observed over the northern polar cap. The time onset of the substorm was determined by the beginning of the compression of the *H*-component for a near midnight auroral station. The three stations selected were College, Leirvogur and Fort Churchill, and data was supported in some doubtful cases from other stations closer to magnetic local midnight.

Fig. 5 shows a histogram of N, the weighted frequency of occurrence of events, plotted against the ratio c_{90}/c_{45} of the counting rates in the 90 degree and 45 degree detectors. The solid curve (N_0) represents the distribution actually measured, and the dotted curve (N_T) is the theoretical distribution calculated under the assumption that the proton intensity at the satellite is isotropic. The overlap between the two histograms were taken on morning and evening polar passes, in the invariant latitude region $\Lambda = 72°$ to $75°$ at a time $T = 0$ hours to 0.5 hours after the substorm expansion. For this example, and all the subsequent ones, we have selected substorms which gave a maximum depression of the *H*-component of the geomagnetic field, at a near local midnight auroral station, of 400 to 600 gammas. Also shown in Fig. 5 is the difference between observed and theoretical histograms, $N_0 - N_T$, and it is this part of the figures which will be

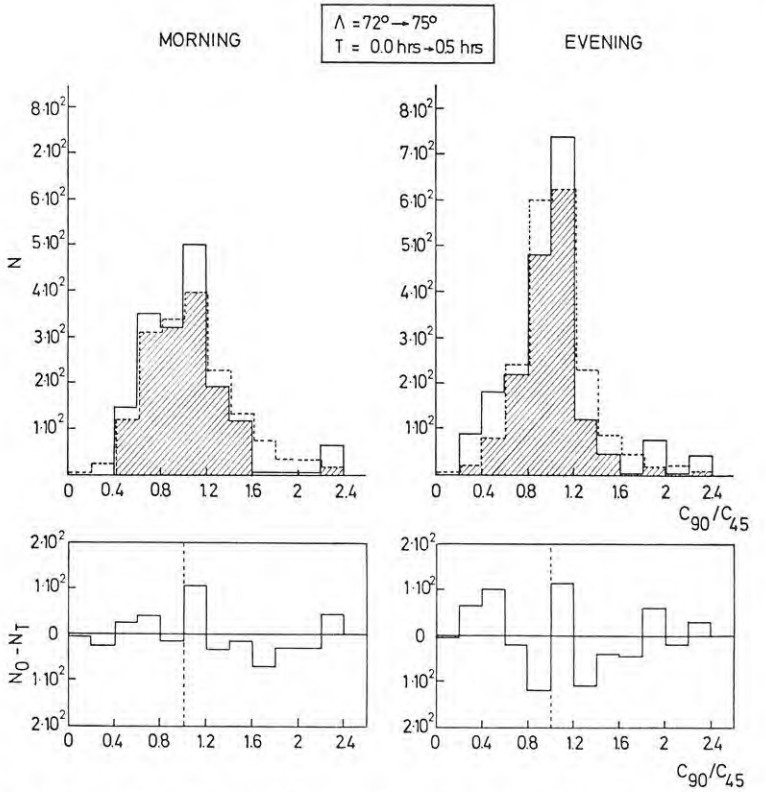

Fig. 5. Histograms of the weighted number of events having $R_0 \leq c_{90}/c_{45} < R$, as function of c_{90}/c_{45}. Solid lines represent the observed distribution, N_0, dotted lines the equivalent theoretical distribution, N_T, if the particle flux is assumed isotropic. The region of overlap is shaded. In the lower panel the difference $N_0 - N_T$ is plotted. Data are shown for morning and evening passes at invariant lat. $\Lambda = 72°–75°$ and at $T = 0$ hours to 0.5 hours after the substorm expansion phase

used to decide whether the measurements are consistent with isotropy, or whether there is evidence for a double loss cone distribution or precipitation. If the observed histogram is shifted towards a lower median c_{90}/c_{45} value with respect to the theoretical curve, this is seen in the N_0—N_T plot as a positive branch at values of c_{90}/c_{45} less than 1, and a corresponding negative branch at c_{90}/c_{45} greater than 1. Such a shift is interpreted as precipitation, i.e. a particle anisotropy where the larger flux mirrors at lower altitudes. Similarly, if the N_0—N_T plot shows a positive branch at values of c_{90}/c_{45} greater than 1 and a negative branch at c_{90}/c_{45} less than 1 we interpret this as a double loss cone or a trapping distribution, since this picture corresponds to the case where the observed histogram has shifted to a larger median value than that of the theoretical histogram.

It is not easy to define meaningful statistical erros for the histograms with which we wish to interpret those magnetospheric processes which influence the particle population. The theoretical histograms themselves are based on and calculated from the measurements (i.e. $\tilde{c}$), so that an observation of a sufficiently large number of events should approximate the theoretical distribution very well. (Obviously a single measurement of c_{90} and c_{45} will produce a complete theoretical histogram, but only a single observational point in one of the 'ratio boxes' $R_0 < \frac{c_{90}}{c_{45}} \leq R$). We have thus compiled Fig. 6, which shows the relative overlap of theoretical and observational histograms as a function of total weighted event number $\sum N_0$

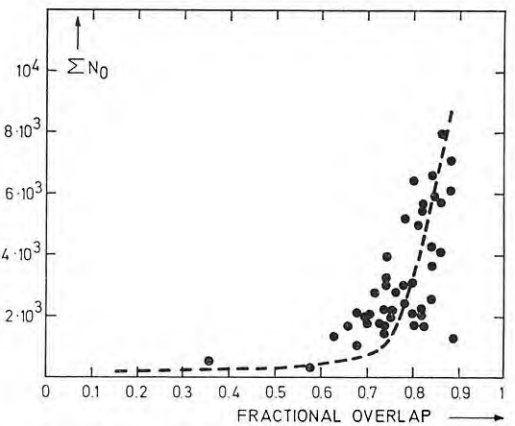

Fig. 6. Relative overlap of theoretical and observational histograms as a function of total weighted event number $\sum N_0$. Data from the open field line region are used for this figure

(i.e. the area under the histogram). As can be seen, for relatively few events the overlap is poor, and it approaches $\sim$100% asymptotically as the total event number increases. This curve was compiled from data points at invariant latitudes where the geomagnetic field lines can be assumed to be open, and at times more than 12 hours away from the substorm expansion phase, i.e. under conditions which should yield isotropic particle distributions. We can use this figure to define a level of $\sum N_0$ above which the number of events is sufficiently large to be able to detect systematic differences between the observed and theoretical histograms over and above the random differences which exist anyway because the event number is finite. This level of $\sum N_0$ is found to be $\sim$1000 by inspection. Fig. 5, for instance, is interpreted as being due to an isotropic distribution, because the fluctuations in N_0—N_T are not systematic.

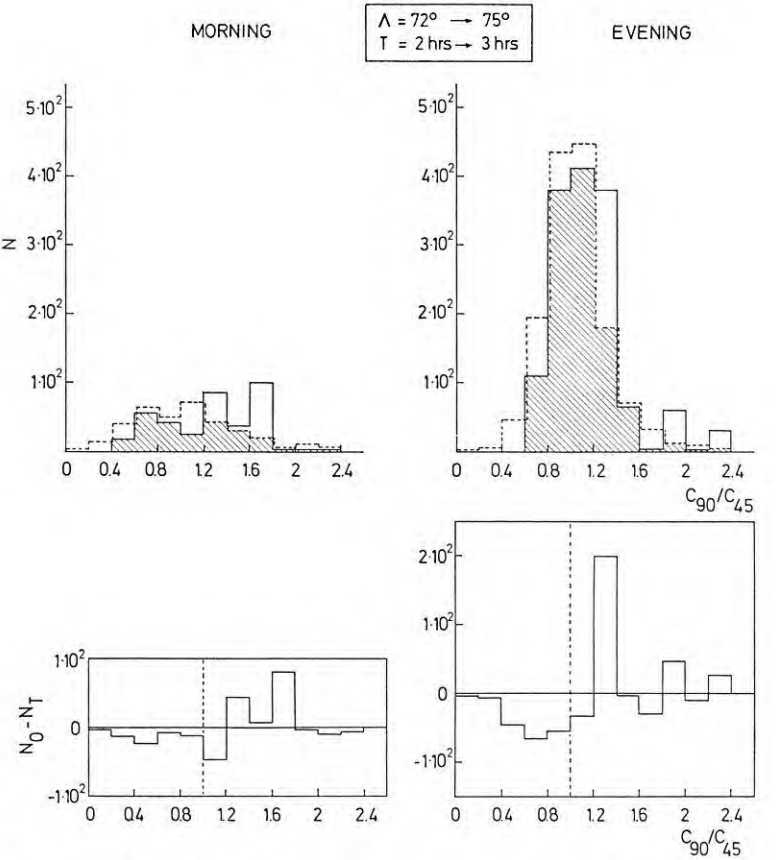

Fig. 7. As for Fig. 5, except that the particle flux exhibits a double loss cone distribution (negative values of $N_0 - N_T$ at $c_{90}/c_{45} < 1$ and positive values at $c_{90}/c_{45} > 1$), and $T = 2$ hrs to 3 hrs after the substorm expansion

Thus in the latitude region just below the last closed field line an isotropic pitch angle distribution (strong pitch angle scattering) is observed at the beginning of the substorm expansion phase.

In this same latitude region, a double loss cone distribution is observed approximately 2 hours after the substorm expansion as can be seen from the positive values of $N_0 - N_T$ for $R > 1$ in Fig. 7. This is due to no or very weak pitch angle scattering, indicating very quiet field conditions.

These observations are in qualitative agreement with measurements of McPherron and Coleman (1970) that enhanced wave-activity occurs just after substorm expansion, and that this period is followed by a magnetically quiet period.

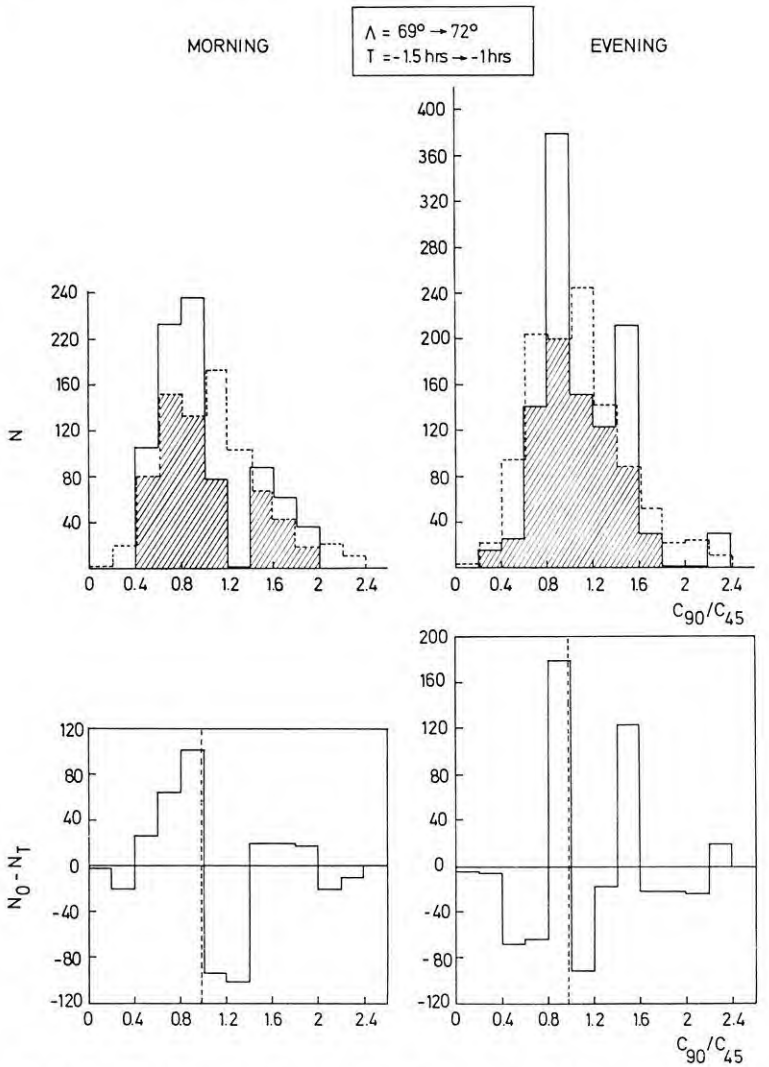

Fig. 8. As for Fig. 5, except that $\Lambda = 69°$—$72°$ and $T = 1.5$ hrs to 1 hr before the substorm expansion phase. Positive values of N_0—N_T at $c_{90}/c_{45} < 1$ are indicative of a precipitating particle flux

At the time of the substorm growth phase onset, energetic proton precipitation was observed in the invariant latitude range 69° to 72°. Fig. 8 shows a sample histogram for this invariant latitude range and referring to a time period approximately 1 hour before the substorm expansion. The systematic differences between the observed (N_0) histogram and the theoret-

ical (N_T) histogram are clearly visible and indicate particle precipitation. Reference to our table shows that the $A = 69°$ to 72° region views the front edge of the neutral sheet during the substorm growth phase.

This unexpected result, i.e. a preferred flow of 1 MeV protons along the geomagnetic field lines, is difficult to understand in terms of wave particle effects occurring near the equator. However, interaction of protons with electron cyclotron waves is coupled with strong energy absorption (Gendrin, 1968) for those particles scattered into small pitch angles, and if such interactions occurred at relatively low altitudes, the observed particle distribution may result.

A quantitative description of the gyroresonant interaction between 1 MeV protons and ion cyclotron and electron cyclotron waves is needed in order to yield the power necessary in the magnetic fluctuations to account for the observations.

Acknowledgement. We are grateful to Dr. G. Haerendel for many helpful discussions.

References

Achtermann, E., Häusler, B., Hovestadt, D., Künneth, E., Laeverenz, P., Paschmann, G.: Die Experimente EI88 and EI93 zur Messung von energiereichen Elektronen, Protonen und Alphateilchen im Satelliten Azur. Rep. BMBW-FBW 70–67, 1970

Aubry, M. P., Russell, C. T., Kivelson, M. G.: On inward motion of the magnetopause before a substorm. J. Geophys. Res. *75*, 7018–7031, 1970

Behannon, K. W.: Geometry of the geomagnetic tail. J. Geophys. Res. *75*, 743–753, 1970

Bewick, A., Haskell, G. P., Hynds, R. J., Morfill, G.: Low energy solar protons in the pseudo-trapping region of the magnetosphere. J. Geophys. Res. *78*, 597–606, 1973

Bewick, A., Haskell, G. P., Hynds, R. J.: Penetration of low energy solar protons to low geomagnetic latitudes. J. Geophys. Res. *75*, 4605–4612, 1970

Blake, J. B., Paulikas, G. A., Freden, S. C.: Latitude intensity structure and pitch angle distributions of low energy solar cosmic rays at low altitude. J. Geophys. Res. *73*, 4927–4934, 1968

Fairfield, D. H., Ness, N. F.: Configuration of the geomagnetic tail during substorms. J. Geophys. Res. *75*, 7032–7047, 1970

Flindt, H. R.: Local time dependence of geomagnetic cut-offs for solar protons $0.52 \leq E_p \leq 4$ MeV. J. Geophys. Res. *75*, 39–49, 1970

Gendrin, R.: Pitch angle diffusion of low energy protons due to gyroresonant interaction with hydromagnetic waves. J. Atmospheric. Terrest. Phys. *30*, 1313–1330, 1968

Häusler, B., Scholer, M., Hovestadt, D.: Variations of the trapped particle population and of cut-off and pitch angle distribution of simultaneously observed magnetospheric solar protons during substorm activity. Submitted to J. Geophys. Res., 1973

Imhof, W.L., Reagan, J.B., Gaines, E.E.: Solar particle cut-offs as observed at low altitudes. J. Geophys. Res. *76*, 4276–4290, 1971

McPherron, R.L., Coleman, P.J.: Magnetic fluctuations during magnetospheric substorms. 1. Expansion phase. J. Geophys. Res. *75*, 3927–3931, 1970

Morfill, G.: A coordinate system for use with high latitude energetic particle phenomena. J. Geophys. Res. *77*, 4010–4020, 1972

Morfill, G.: Nonadiabatic particle motion in the magnetosphere. J. Geophys. Res. *78*, 588–596, 1973a

Morfill, G.: Solar particle access into the inner magnetosphere. Preprint, 7. ESLAB Symposium, Saulgau, Germany, 1973b

Ness, N.F., Williams, D.J.: Correlated magnetic tail and radiation belt observations. J. Geophys. Res. *71*, 322–325, 1966

Paulikas, G.A., Blake, J.B., Freden, S.C.: Low energy solar cosmic ray cut-offs: diurnal variations and pitch angle distributions. J. Geophys. Res. *73*, 87–95, 1968

Paulikas, G.A., Blake, J.B., Vampola, A.L.: Solar particle observations over the polar caps. In: Intercorrelated satellite observations related to solar events. (V. Manno and D. E. Page, eds) Dordrecht-Holland, 1970

Roberts, C.S.: Pitch angle diffusion of electrons in the magnetosphere. Rev. Geophys. *7*, 305–337, 1969

Schindler, K., Ness, N.F.: Internal structure of the geomagnetic neutral sheet. J. Geophys. Res. *77*, 91–100, 1972

Williams, D.J., Heuring, F.T.: Strong pitch angle diffusion and magnetospheric solar protons. J. Geophys. Res. *78*, 37–50, 1973

Williams, D.J., Ness, N.F.: Simultaneous trapped electron and magnetic tail field observations. J. Geophys. Res. *71*, 5117–5128, 1966

Dr. Manfred Scholer
Dr. Gregor Morfill
Dr. Dieter Hovestadt
Max-Planck-Institut für Physik
und Astrophysik
Institut für extraterrestrische Physik
D-8046 Garching bei München
Federal Republic of Germany